American Mineralogist, Volume 94, pages 210–221, 2009

Suhailite, a new ammonium trioctahedral mica

María Dolores Ruiz Cruz[1,*] and Carlos Sanz de Galdeano[2]

[1]Departamento de Química Inorgánica, Cristalografía y Mineralogía, Universidad de Málaga, 29071 Málaga, Spain
[2]Instituto Andaluz de Ciencias de la Tierra, CSIC-Universidad de Granada, 18071 Granada, Spain

Abstract

A new ammonium-bearing trioctahedral mica (suhailite) has been found in gneisses from the Betic Cordillera (Spain). Suhailite appears as aggregates of golden grains unoriented with respect to the main foliation. It shows weak pleochroism from light to darker yellow and low birefringence (0.028). X-ray data indicate the presence of two compositional variations: a NH_4-rich phase (with a basal spacing of 10.40–10.44 Å) and a NH_4-K intermediate phase (with basal spacing of 10.20–10.26 Å). Average composition, as deduced from analyses obtained at the scale of the scanning electron microscope is $[Ca_{0.04}Na_{0.07}K_{0.35}(NH_4)_{0.55}](Al_{0.42}Ti_{0.22}Fe_{1.33}Mn_{0.01}Mg_{0.71})_{\Sigma=2.70}(Si_{2.67}Al_{1.33})O_{10}(OH)_2$. Thermal data indicate that maximum NH_4 detachment occurs at 502 °C, suggesting a thermal stability similar to tobelite. Textural data indicate that unoriented golden grains consist of fine intergrowths of annite and suhailite and suggest that suhailite formed from primary red annite during the annite to fibrolite transformation.

Keywords: Annite, Betic Cordillera, suhailite, SEM, TEM/AEM, XRD

Introduction

The presence of ammonium in the interlayer space of micas has been documented for many years (Vedder 1964; Honma and Itihara 1981; Honma 1996; Mingram and Braüer 2001). Nevertheless, whereas dioctahedral mica and illite with high ammonium content (tobelite) have been identified in low-temperature environments (<300 °C) (e.g., Higashi 1982; Juster et al. 1987; Daniels and Altaner 1990; Nieto 2002), ammonium-rich trioctahedral micas have not been observed as naturally occurring minerals, despite the fact that trioctahedral ammonium mica (ammonium phlogopite) has been repeatedly synthesized in laboratory experiments (Eugster and Muñoz 1966; Boss et al. 1988; Harlov et al. 2001).

Tobelite formed at higher temperature (>400 °C) has been described for the fist time by Ruiz Cruz and Sanz de Galdeano (2008) in deep schists of the Alpujárride Complex (Internal Zone of the Betic Cordillera). Tobelite, although widespread through the cordillera, only persists as scarce relics in some graphite-rich microdomains, defining the first schistosity. Textural relations indicate that this mica formed during an older pre-Alpine metamorphic episode. Finding of tobelite in Alpujárride mica schists led us to perform a detailed sampling and study of micas from gneisses underlying the schist formations. This study revealed that NH_4^+-bearing annite [with NH_4^+ content on the order of 0.10 atoms per formula unit (apfu)] is a common constituent of the deep formations of this complex. In addition, NH_4-richer annite was locally found. We describe here this new term of the biotite series, for which the name suhailite has been recently approved by the Commission on New Minerals, Nomenclature and Classification of the IMA.

A sample (cotype) has been deposed at the Museo Nacional de Ciencias Naturales of Spain, with catalog number: MNCN 26418.

* E-mail: mdruiz@uma.es

Occurrence

Although ammonium-bearing annite is widespread along the Betic Cordillera (South of Spain), suhailite has been identified in a more restricted area, located at the Fuengirola-Coín road (N36° 33′ 9.6″ – W4° 41′ 20″), in the Málaga province. This area was extensively sampled but suhailite-bearing samples are limited to a small outcrop. Suhailite has also been identified in gneisses from the Rif, although these data are not included here.

Suhailite has been found in polymetamorphic pelitic gneisses and transitional schists-gneisses from the uppermost tectonic unit of the Alpujárride Complex. These formations consist of thick sequences of dark mica schists and gneisses, which have been generally ascribed to the lower Paleozoic or even the Precambrian (Egeler and Simons 1969). A low-temperature/high-pressure Alpine metamorphism, overprinted by a high-temperature/low-pressure one has been described in these units (García-Casco et al. 1993; Azañón et al. 1997). The effect of the earlier Hercynian episode, identified more recently (Zeck and Whitehouse 1999, 2002), has been, in contrast, scarcely investigated.

Appearance and physical properties

Suhailite appears as golden grains with variable size (50 μm–0.1 mm). Determination of the physical properties of suhailite is hindered by the grain size and by the presence of abundant graphite inclusions. The megascopic color and the streak are golden, and the luster pearly. It is translucent and the hardness (Mohs) = 2.5. It shows a perfect {001} cleavage. The density, calculated from the chemical data obtained at the scale of the scanning electron microscope is 2.954 g/cm^3, and that calculated based on the chemical data obtained at the scale of the transmission electron microscope is 2.920 g/cm^3.

Petrography and optical properties

Suhailite-bearing gneisses contain mica fractions dominated by annite with minor suhailite. Early, red-to-brown annite grains

0003-004X/09/0203–210$05.00/DOI: 10.2138/am.2009.3008

show parallel orientation and are extensively replaced by fibrolite (Figs. 1a and 1b); suhailite appears, in contrast, as later, generally unoriented golden grains with abundant graphite inclusions (Fig. 1b). Although the suhailite content is generally low, it appears concentrated in some graphite-rich areas, forming aggregates (up to 1 mm long) of grains (50–100 μm), subparallel to the bands defined by the oriented grains of annite and sillimanite. Nevertheless, obtaining mica-enriched separates is very difficult, since the mica content in the rocks is generally very low (~10%) and it appears intimately intergrown with other phases.

Associated minerals, in order of decreasing abundance, are quartz, plagioclase (oligoclase-andesine), orthoclase, annite, sillimanite (fibrolite), garnet, graphite, ilmenite, rutile, tourmaline, chlorite, vermiculite, smectite, and kaolinite, these latter three phases being retrogressive replacement minerals (Figs. 1c and 1d). Muscovite and Na-bearing trioctahedral mica are occasionally present in minor amounts.

Suhailite is biaxial (–), with α = 1.624 (0.002), β = 1.652 (0.002), γ = 1.652 (0.002), and 2*V* (measured): 0–4° (1)°. It does not show dispersion. The orientation is $\alpha \wedge Z \sim 3°$, β // Y. Suhailite shows pleochroism from colorless or light yellow (α) to light yellow or dark yellow (β and γ).

X-ray data

X-ray diffraction (XRD) patterns were recorded using a Philips X'Pert PRO MPD (University of Málaga), with Cu$K\alpha_1$ radiation and Ge monochromator, operated at 40 mA and 40 kV. XRD patterns were obtained from both unoriented and oriented samples. XRD patterns used for cell refinement were obtained with 0.017° step size and counting time of 800 s. The XRD patterns of the oriented samples were obtained with 0.017° step size and counting time of 50 s. Oriented samples were prepared by sedimentation, after ultrasonic dispersion. The patterns were obtained in the air-dried state, after treatment with ethylene-glycol and after heating at increasing temperatures (100–550 °C). Additional XRD patterns were obtained after K-saturation and heating at 150 °C (Drits et al. 1997, 2005). The XRD patterns of air-dried samples show a broad ~10 Å reflection (Fig. 2a), which includes three main reflections, interpreted as corresponding to micas with increasing NH_4 contents (Drits et al. 1997): annite (basal spacing of ~10.04 Å), an intermediate, K-rich suhailite (with basal spacing ranging from 10.20 to 10.26 Å), and suhailite (basal spacing ~10.44 Å) (Fig. 3a). A reflection at ~11 Å, interpreted as due to partially hydrated mica, is also occasionally present. Annite is the most abundant mica, followed by the mica with intermediate composition, whereas the NH_4-richest mica is present in lower amounts. Estimation of the annite:intermediate mica:suhailite ratio (Fig. 2b) was carried out after fitting the experimental peaks, and using the patterns simulated with WinStruct, based on the chemical data shown below; nevertheless, given the low suhailite content in most samples, the deduced ratios must be considered as approximate values. The higher order basal reflections of NH_4-micas are weak (Fig. 2a) but some of these (003, 004, and 005) can be identified in the patterns of samples with the highest suhailite contents (Figs. 3b–3c). A good agreement between experimental and simulated patterns was observed, except for the intensity of the 004 suhailite reflection, which is higher than expected, assuming that the intermediate mica and suhailite have similar silicate layer composition. Increase in intensity of the 004 reflection could be due either to contribution of the 200 reflection of the intermediate mica or to compositional differences between both micas. On the basis of the several simulated patterns, an increase in the relative intensity of the 004 reflection could be due to a higher Fe/(Fe + Mg) ratio in the NH_4-richest mica. Because the relative intensity of the ammonium-bearing mica reflections is very low, as compared with those of annite (Fig. 2b), the more useful reflection for identification of ammonium-mica is the 001. Although the basal reflections corresponding to the three mica types can be differentiated in some suhailite-bearing samples (Fig. 2a), refinement of the cell parameters of suhailite is hindered by the presence of quartz, feldspars, and sillimanite, and especially by the presence of annite and the more abundant intermediate mica. Table 1 shows the more important reflections of the three mica types and Table 2 the deduced unit-cell parameters, refined

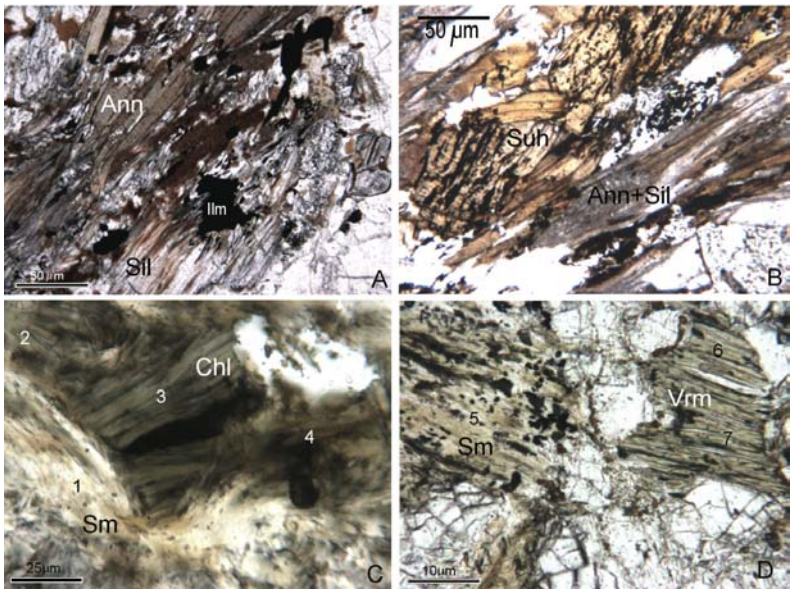

FIGURE 1. Microscopic images of annite, suhailite and retrogressive phases. (**a**) Subparallel grains of red annite extensively replaced by sillimanite (fibrolite) from sample MP-1. (**b**) Unoriented grains of graphite-rich golden suhailite from sample MP-1. (**c**) Grains of green retrogressive chlorite and possible chlorite/vermiculite intermediate phases from sample MP1-5. (**d**) Smectitic and vermiculitic phases (probably chlorite/vermiculite mixed-layers) from sample RMP1-1. Mineral symbols according to Kretz (1983) except for suhailite (Suh). Numbers in **c** and **d** correspond to analyses in Table 5. All photomicrographs with parallel nicols.

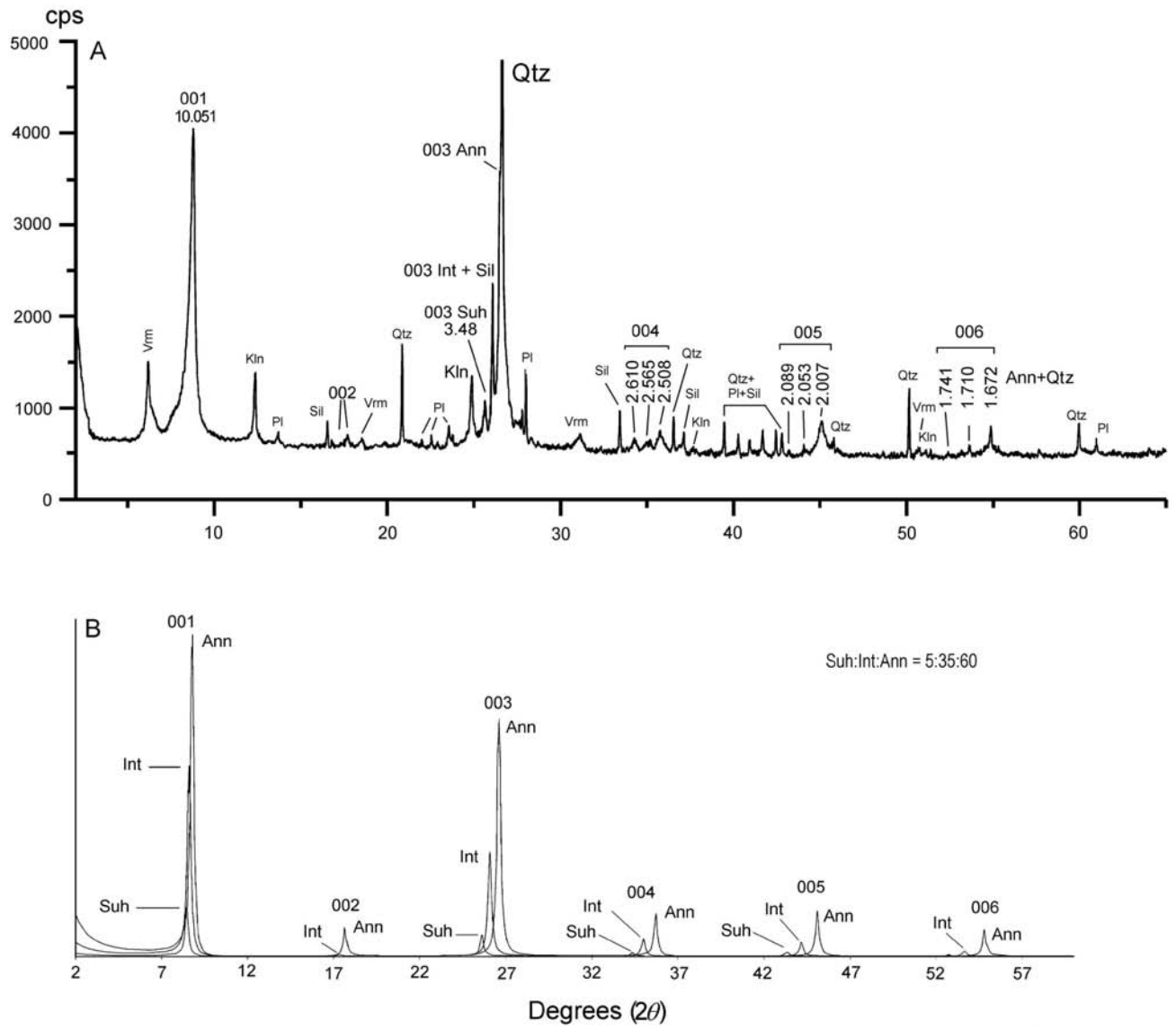

FIGURE 2. (**a**) XRD pattern of an oriented, air-dried suhailite-bearing sample (RMP1-2M). Other phases present are quartz, plagioclase, sillimanite, kaolinite, and vermiculite. (**b**) Simulated pattern of a mixture (60:35:5) of annite, intermediate mica, and suhailite.

for annite and the intermediate mica, and calculated from the more intense reflections for suhailite. The results of the refinement of the cell parameter of annite, obtained from a suhailite-free sample, and of the intermediate mica from the sample with the highest relative NH_4-mica content (sample MP-1M, Table 3) are shown in Appendix 1.[1]

Treatment with ethylene-glycol (at 60°) reveals that the first mica peak does not appreciably change with glycolation. K-saturation and heating at 150 °C causes some modifications

TABLE 1. Main reflections of annite, intermediate NH_4-K mica, and suhailite (sample MP-1)

Annite		Int. mica		Suhailite			
d	*I*	*d*	*I*	*d*	*I*	I_{total}	*hkl*
10.049	100	10.242	100	10.44	100		001
5.067	15	5.121	8	5.220	5		002
4.600		4.600		4.600		4	020
4.579		4.540		4.540		4	110
3.345	100	3.414	46	3.485	30		003
2.679		2.644		2.644		11	130
2.507	10	2.561	8	2.613	8		004
2.008	18	2.048	5	2.088	8		005
1.542	23	1.533		1.533		6	060

TABLE 2. Cell parameters deduced for annite, NH_4-K intermediate mica, and suhailite

Red annite	Intermediate mica	Suhailite
a = 5.349 (0.004) Å	a = 5.296 (0.003) Å	
b = 9.237 (0.006) Å	b = 9.199 (0.005) Å	b = 9.199 Å
c = 10.202 (0.007) Å	c = 10.412 (0.006) Å	$c\sin\beta$ = 10.447 Å
β = 99.999 (0.05) (°)	β = 99.991 (0.05) (°)	
V = 496.47 (0.53) Å^3	V = 499.56 (0.50) Å^3	

[1] Deposit item AM-09-009, Appendix 1 and 2. Deposit items are available two ways: For a paper copy contact the Business Office of the Mineralogical Society of America (see inside front cover of recent issue) for price information. For an electronic copy visit the MSA web site at http://www.minsocam.org, go to the American Mineralogist Contents, find the table of contents for the specific volume/issue wanted, and then click on the deposit link there.

TABLE 3. Lithology, mineral assemblages, C and N contents in whole rocks or mica concentrates (M) of samples from the Fuengirola outcrop

Sample	Lithology	Mineralogy	C (wt%)	N (wt%)	Mica (wt%)	Ms:An:Suh	Suh (wt%)	NH_4 (wt%) in Suh*
MP-1M	Gneiss	Qtz + Pl + Or + Ky + Sil + Ann + Suh + Vrm + Kln	1.49	0.123	18	0:63:37	6.7	2.37
MP-1-1	Gneiss	Qtz + Pl + Or + Sil + Ann + Suh + Vrm + Kln	0.54	0.023	10	0:62:38	3.8	0.78
MP-1-3M	Gneiss	Qtz + Pl + Or + Sil + Ms + Ann + Suh + Vrm + Kln	1.25	0.087	39	52:31:17	9.2	1.69
MP-1-4M	Gneiss	Qtz + Pl + Or + Sil + Ms + Ann + Suh + Vrm + Kln	1.64	0.038	16	2:82:16	2.6	1.88
MP-1-5M	Gneiss	Qtz + Pl + Or + Sil + Ann + Suh + Vrm + Kln	0.68	0.027	13	0:87:13	1.7	2.04
RMP1-1	Gneiss	Qtz + Pl + Sil + Ann + Suh + Vrm + Kln	0.19	0.010	7	0:81:19	0.8	0.97
RMP1-2M	Gneiss	Qtz + Pl + Sil + Ann + Suh + Tur + Vrm + Kln	0.72	0.017	10	0:59:41	4.5	0.53
RMP1-3	Schist	Qtz + Pl + Or + Sil + St + Ann + Suh + Vrm + Kln	0.88	0.009	24	0:83:17	4.1	0.28
RMP1-4	Gneiss	Qtz + Pl + Or + Sil + Ms + Ann + Suh + Chl	2.24	0.023	32	10:76:14	4.5	0.66
RMP1-5M	Gneiss	Qtz + Pl + Or + Sil + Ms + Ann + Suh + Vrm + Kln	1.27	0.051	26	3:89:8	3.1	3.15
RMP1-6	Schist	Qtz + Pl + Sil + St + Gt + Ms + Ann + Vrm + Kln	0.31	0.012	62	82:15:3	1.9	0.83
RMP1-7	Schist	Qtz + Pl + Sil + St + Ky + Ms + Ann + Vrm + Kln	1.13	0.011	73	90:8:2	1.5	0.97

Note: Muscovite:annite:suhailite ratios and deduced NH_4 contents in suhailite are also included.
* Including the end term and the mica with intermediate composition

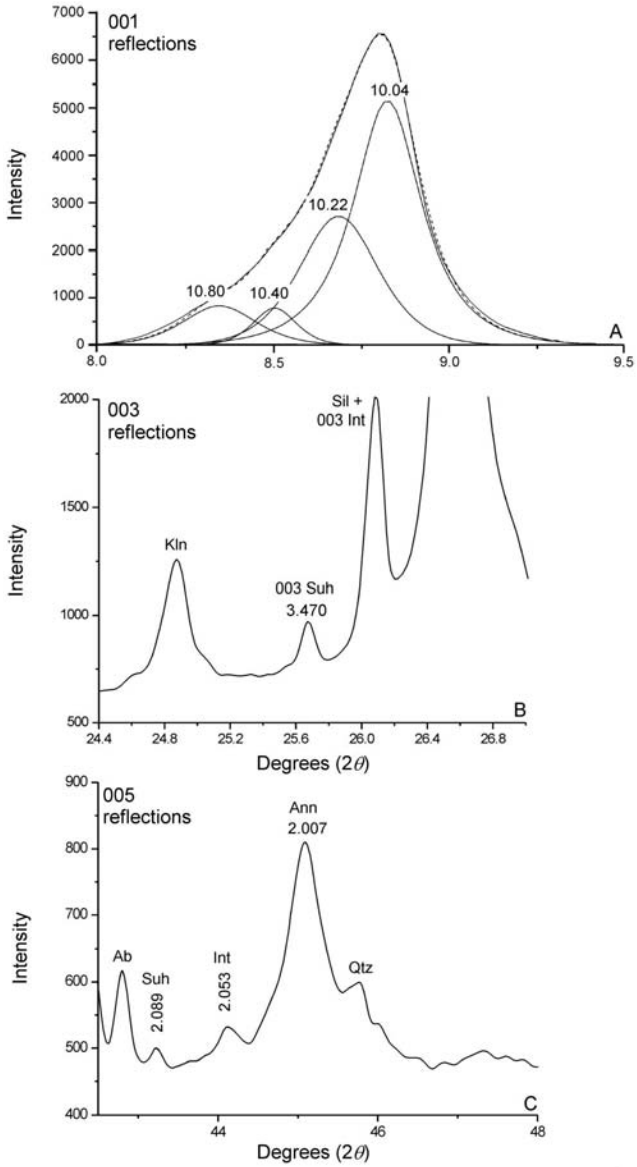

◀**FIGURE 3.** Selected zones of the XRD pattern shown in Figure 2. These patterns have been smoothed for eliminating the background. (**a**) Region of the 001 reflections and decomposition of the peak. (**b**) Region of the 003 reflections. In this range, the reflection of the intermediate mica overlaps with that of sillimanite and the reflection of suhailite with that of plagioclase. (**c**) Region of the 005 reflections. The shape of the annite reflection indicates the presence of annite with variable NH_4 contents.

in position and relative intensity of the several reflections (Figs. 4a and 4b). The most evident is the increase in intensity of the ~10 Å reflection, due to the contribution of the contracted 001 reflection of vermiculite, and perhaps of a fraction of the ~11 Å reflection (hydrated K-mica). In addition, a slight shift and increase of the relative intensity of the ~10.4 Å reflection with respect that of the intermediate mica is probably due to the contribution of a fraction of the contracted ~11 Å reflection (hydrated NH_4-mica). Heating between 100 and 300 °C (Figs. 5a and 5b) causes the complete contraction of the vermiculite reflection (not shown) as well of the reflection ascribed to hydrated mica, again accompanied by the increase in intensity of the 10 Å reflection. In contrast, suhailite reflections maintain their intensity up to 500–550 °C, although a clear shift toward lower spacings is observed from ~400 °C (Figs. 5c and 5d). The behavior of the basal reflections after K-saturation and heating at increasing temperatures suggests that the ammonium-bearing mica does not contain appreciable amounts of vermiculite or smectite-like layers, and that ammonium detachment begins at about 400 °C.

CHEMICAL DATA

Because sufficient amounts of suhailite could not be obtained for wet chemical analysis, the chemical characterization was carried out by electron microprobe (EMPA), X-ray energy dispersive (EDX), and analytical electron microscopy (AEM). The results presented here are mainly based on the EDX and the AEM analyses since EMPA data are hindered by rapid NH_4 volatilization.

Estimation of the average NH_4 content in suhailite was determined by combining elemental analysis of total N contents (Schroeder and Ingall 1994) with XRD-based estimates of approximate muscovite:anninte:suhailite ratio in the samples. Elemental analysis was performed with an 1108 (Carlo Erba) CHN analyzer (University of La Coruña). Analysis conditions were: Oxidation temperature = 1020 °C; reduction temperature = 650 °C; $P(O_2)$ = 100 KPa. The standard used was sulfanilamide (BBOT). The detection limit is 0.001 wt%. Replicate analyses

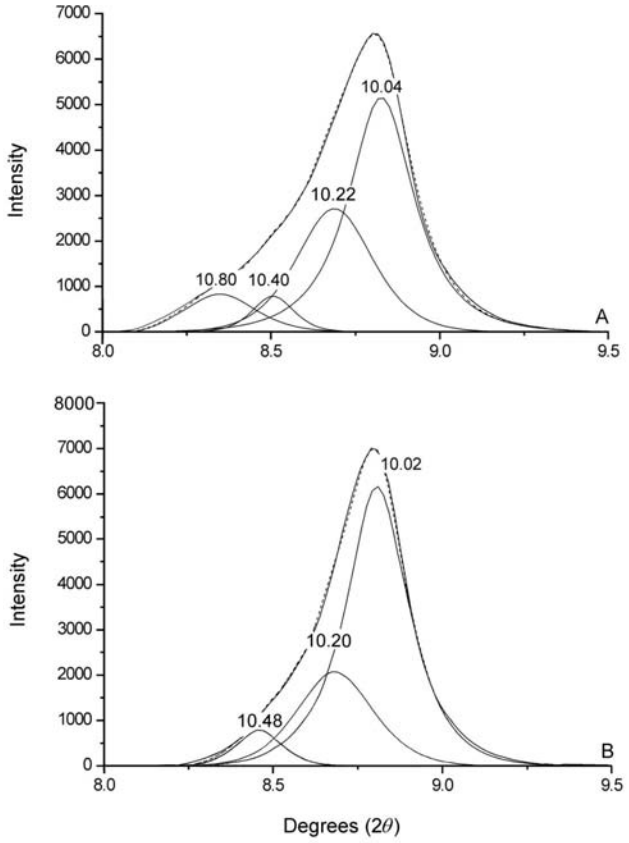

FIGURE 4. XRD patterns of the 001 2θ region of micas (sample RMP1-2M), showing the behavior of the basal reflections after K-solvation and heating at 150 °C. The sample also contains partially hydrated mica (reflection at ~10.8 Å).

indicate that the error in N determination is <0.005%.

Nitrogen contents in whole rocks and mica concentrates of samples are reported in Table 3. The approximate muscovite:anninte:suhailite ratios are also reported in Table 3. The variations observed in calculated NH_4 content in micas (0.28–3.15 wt%) probably derive from both true variations in NH_4 contents between gneisses and overlying schists and from inaccuracy in estimation of the suhailite contents.

SEM results

SEM data were collected on a ZEISS DSM 950 scanning electron microscope (SEM), equipped with an EDX system (LINK QX 2000) (Universidad de Granada). Working conditions for the SEM/EDX analyses were accelerating voltage of 14 kv, 2 nA beam current, and beam diameter of 0.5 µm. Standards were albite (Na), orthoclase (K), periclase (Mg), wollastonite (Si and Ca), and synthetic oxides (Al_2O_3, Fe_2O_3, and $MnTiO_3$).

Numerous analyses of annite and suhailite were obtained using the SEM/EDX. Because many suhailite grains have undergone retrograde reactions to vermiculitic phases and these replacement phases and suhailite are characterized by a low content of Na + K + Ca, two types of samples were used for suhailite characterization. In addition to the less altered samples, also used for structural refinements and other determinations (MP-1 and MP-1-1), retrograde samples (e.g., MP1-5, RMP1-1) were analyzed to accurately characterize the chemical modifications due to retrogression. In addition to the chemical data described below, suhailite and vermiculite can be generally differentiated in the back-scattered images, based on the presence of oriented graphite inclusions in suhailite (Fig. 6a), the contraction of vermiculite against the electron beam, and the presence of large rutile inclusions in vermiculite (probably formed during trans-

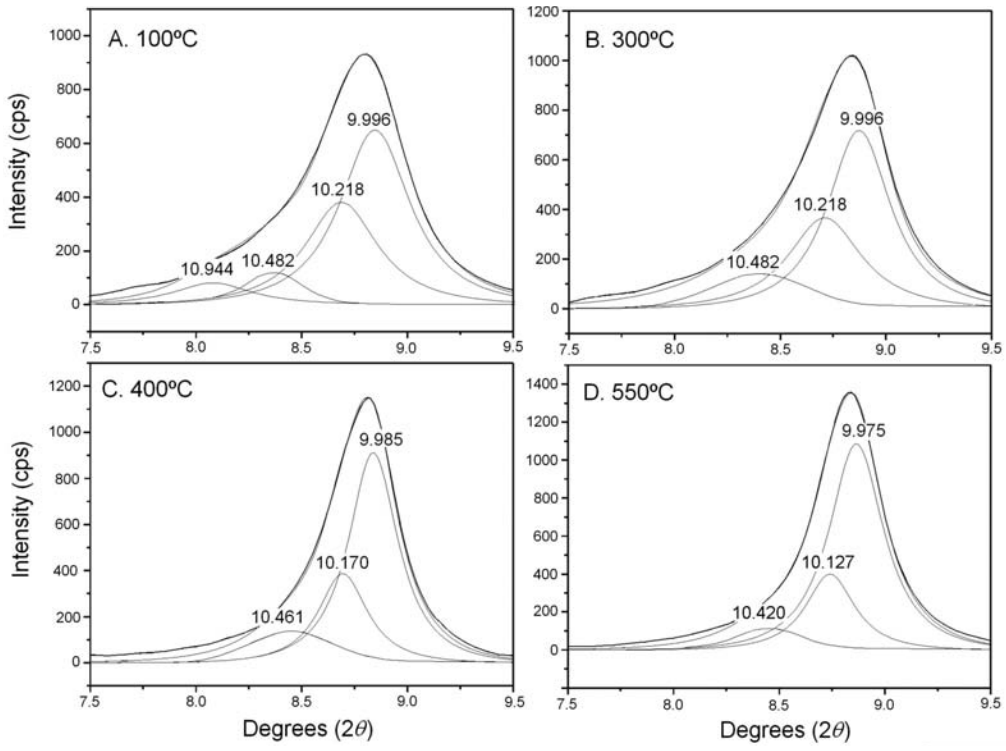

FIGURE 5. XRD patterns of the 001 reflections of micas, showing their behavior at increasing temperatures (Sample RMP1-1). This sample also contains partially hydrated mica (reflection at ~11 Å).

formation of mica into vermiculite; Fig. 6b).

Useful chemical plots (Fig. 7) were constructed from the atomic percent data, including Ti vs. Si (Fig. 7a), Fe + Mg vs. Si (Fig. 7b), Fe + Mg vs. Al (Fig. 7c), and Ca + Na + K vs. Fe + Mg (Fig. 7d). In these plots, the products of mica transformation define two different chemical trends: (1) transformations into dioctahedral phases (mainly kaolinite and smectite) are characterized by an increase of Si and Al, and decrease of Fe + Mg; and (2) transformations into trioctahedral phases (vermiculitic and chloritic phases) are characterized by an increase in Fe + Mg, and decrease in Si. On the Ti vs. Si plot (Fig. 7a) the alteration products are characterized by the notable decrease in Ti relative to the parent mica phase. Excluding the analyses contaminated by alteration products kaolinite, smectite, chlorite or vermiculite, micas are observed to occupy a restricted compositional field in the chemical plots (Fig. 7). Three mica populations were discerned, based on their microscopic color: The first one, corresponding to red annite grains, has high Na + K + Ca and Ti contents. The second population, corresponding to brownish grains, has intermediate Na + K + Ca contents and is interpreted as corresponding to annite grains partially transformed into suhailite. Finally, the third population, with low but more variable Na + K + Ca contents, corresponds to golden grains. Decreasing Na + K + Ca contents are interpreted, on the basis of the XRD data and the elemental analyses, as due to increasing NH_4 contents. For estimating the NH_4 content from the EDX data, we have calculated the formulae on the basis of $O_{10}(OH)_2$ and assuming an interlayer occupancy = 1 apfu (Ruiz Cruz and Sanz de Galdeano 2008). The main disadvantage of this method is that the possible existence of the $K^{IV}Al_{-1}Si_{-1}$ pyrophyllite vector is not considered, i.e., we consider a complete interlayer occupancy. Nevertheless, these results agree with the NH_4 contents deduced from elemental analyses, indicating that this calculation is a good approximation.

The chemical plots based on the calculated formulae, after removing the analyses of grains with intermediate optical properties (Fig. 8), reveal that annite and suhailite define two chemical trends that converge at high Si contents (Fig. 8a). The NH_4 content in suhailite is homogeneous at the grain scale but shows important variation from grain to grain. Maximum NH_4 content is 0.74 apfu. Although the XRD data indicate the presence of a NH_4-rich phase, it seems possible that this phase can hold important amounts of K. Figure 8b reveals a clear negative correlation between Si and Fe + Mg in both annite and suhailite, the Si-poorer (and NH_4-richer) grains showing the highest Fe + Mg contents. Table 4 reports the average EDX analyses of suhailite and annite, which show a strong chemical similarity between these phases except for the NH_4 content. Nevertheless, there are some other differences. Figure 8c reveals that the Ti content is lower in suhailite. In addition, the Ti content measured at the SEM scale includes submicroscopic rutile inclusions, which were only observed by TEM (see below). Another significant trend, shown in Figure 8d, is the exponential increase of the Fe concentration with increasing Fe + Mg contents in suhailite, which could explain the higher intensity of the 004 reflection in the experimental patterns, relative to the simulated ones, as discussed above. Table 5 reports some representative analyses of the retrogressive phases shown in Figures 1 and 6.

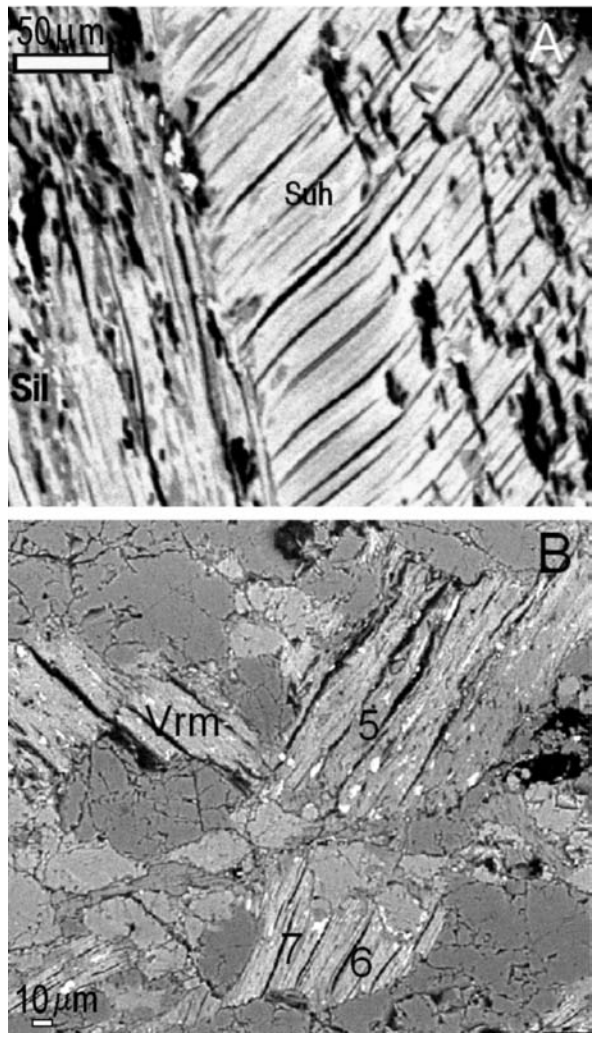

FIGURE 6. Back-scattered images of suhailite and retrogressive phases. (**a**) Image of a suhailite grain from sample MP-1. (**b**) Smectitic and vermiculitic phases from sample RMP1-1, showing important contraction under the electron beam and presence of abundant rutile inclusions. Numbers in **b** correspond to analyses in Table 5.

The complete set of EDX analyses of the micas is reported in Appendix 2.[1]

EMPA study

Numerous grains were analyzed by EMPA. Analyses were obtained with a Cameca SX100 in the CIC (Granada University). EMPA analyses required a previous calibration of N using the two available standards (BN), supplied by Cameca and SPI. The beam diameter was 10 µm with accelerating voltage of 15 kV and variable beam current and counting times of N. The data were reduced using the X-PHI correction. Standards were albite (Na), periclase (Mg), synthetic SiO_2 (Si), Al_2O_3 (Al), TiO_2 (Ti), Fe_2O_3 (Fe), Cr_2O_3 (Cr), NiO (Ni), $MnTiO_3$ (Mn), sanidine (K), and diopside (Ca).

Microprobe analysis of NH_4 is, however, hindered by numerous problems, the main one being the rapid volatilization of N. Our analyses lead systematically to low totals and interlayer occupancies <1 apfu. Some of these analyses are reported in

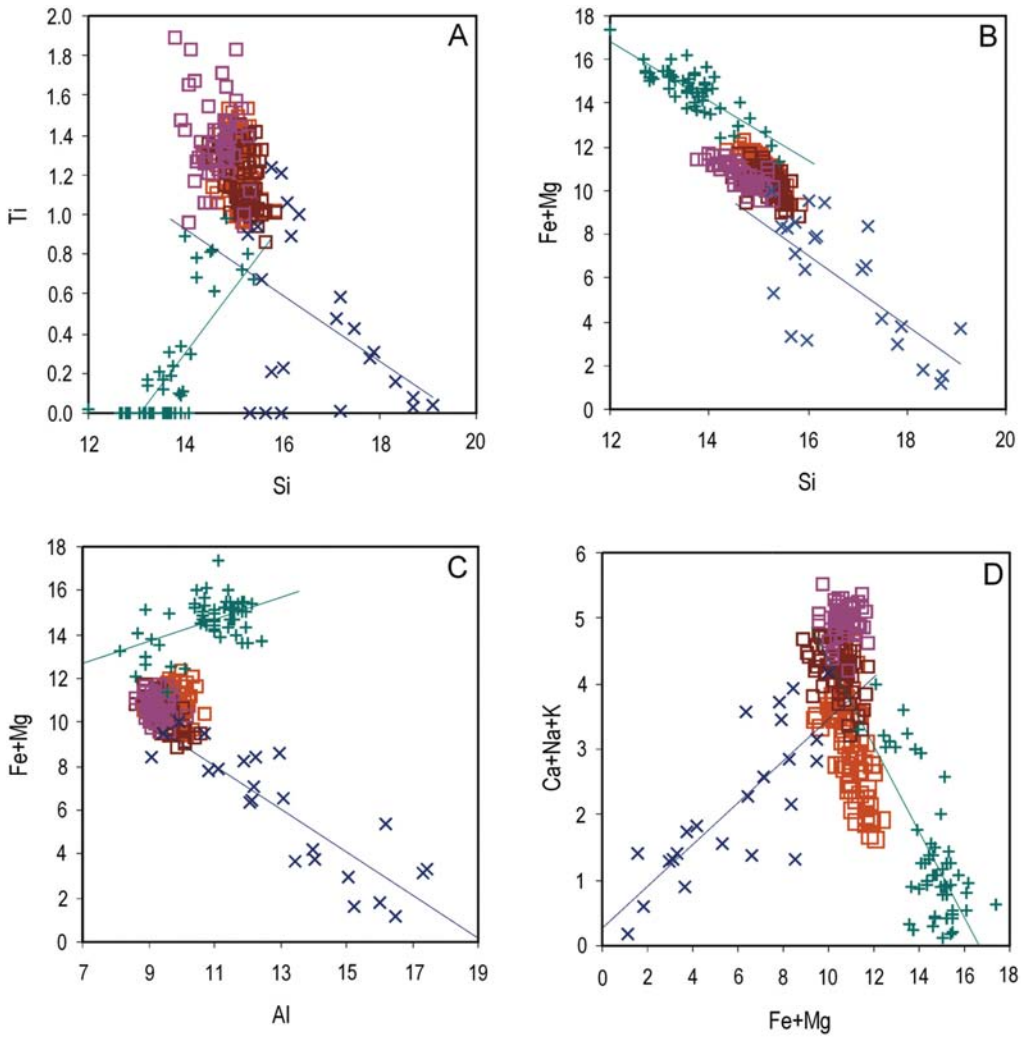

FIGURE 7. Selected EDX chemical diagrams (at%), showing the fields of annite (violet squares), suhailite (orange squares), micas with intermediate optical properties (brown squares), retrogressive phases, and mica grains contaminated by retrogressive phases: dioctahedral phases (blue crosses); trioctahedral phases (green crosses). The chemical trends defined by retrogressive phases have been drawn.

Table 6. As compared with the average formula deduced from the EDX analyses, EMPA formulae show higher Si, as a consequence of the unrealistically low interlayer occupancy. The chemical trends are, however, similar to those deduced from the EDX data. Despite the very low measured NH_4 contents, a curious chemical trend is the positive correlation observed between NH_4 and Cl, which also permits differentiation between annite and suhailite (Fig. 9).

Although very little attention has been devoted to Cl substitution for (OH) in biotite, it is generally considered (Guidotti 1984 and references therein) that Cl in metamorphic micas is directly inherited from the pre-metamorphic protolith, as also assumed here. The Cl content in red annite is generally <0.05 (wt%), whereas it increases considerably in suhailite (up to 0.48 wt%), suggesting that Cl was inherited from the precursor mica, and that enrichment occurred during transformation of red annite into suhailite.

TEM/AEM study

Grains of red annite and suhailite, selected from thin sections, were ion-thinned for transmission-analytical electron microscopy (TEM-AEM). This study was carried out with two main objectives: (1) interpretation of variations in chemical composition among different suhailite grains, and (2) evaluation of possible intergrowths or interstratifications with chlorite and/or vermiculite.

AEM data were collected on a Philips CM-20 TEM, operated at 200 kV and fitted with a scanning transmission device and solid-state detector for energy-dispersion analysis (Universidad de Granada). Microanalyses were obtained in STEM mode. Quantitative determinations used the thin-film approximation of Cliff and Lorimer (1975). Albite (Na), muscovite and annite (K), albite, spessartine and muscovite (Al), forsterite and annite (Mg and Fe), spessartine (Mn), and titanite (Ca and Ti) were used as standards. TEM images with higher resolution were obtained in a Jeol 3000 F, operated at 300 kV (University Complutense, Madrid).

The TEM-AEM study showed that annite grains are composed of thick packets where the regularity is only interrupted by the 00*l* cleavage planes (Fig. 10a). The SAED patterns indicate the presence of one-layer and two-layer ordered polytypes. Some annite grains are replaced by retrograde chlorite (Fig. 10b). In

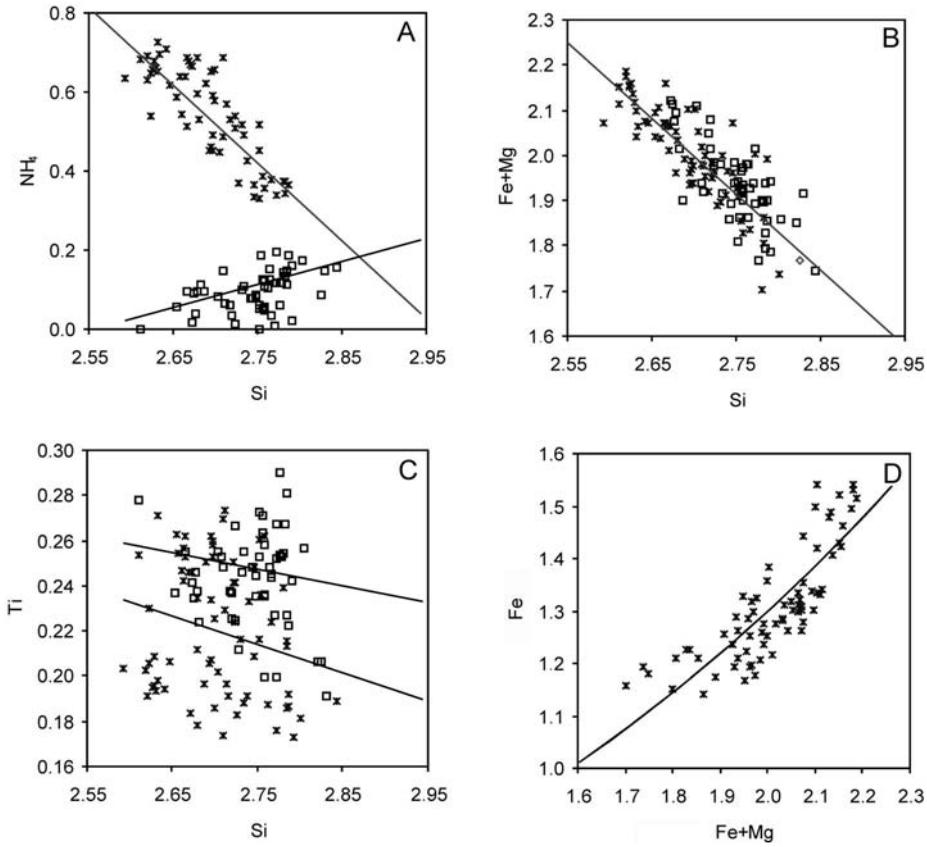

FIGURE 8. NH_4 vs. Si (**a**), Fe + Mg vs. Si (**b**), and Ti vs. Si plots (**c**) (apfu), showing the chemical trends defined by annite and suhailite. The Fe vs. Fe + Mg plot (**d**) shows the exponential increase of Fe at increasing Fe + Mg contents in suhailite. Diamonds = suhailite; squares = annite.

TABLE 4. Average composition of suhailite and coexisting red annite

	Red annite EDX		Golden suhailite EDX		Golden suhailite AEM	
	Average (52)	σ	Average (63)	σ	Average (30)	σ
SiO_2	35.81	0.85	35.77	0.63	38.42	0.82
Al_2O_3	19.11	0.62	19.93	0.74	20.64	0.43
TiO_2	4.34	0.30	3.97	0.51	2.39	0.24
FeO	21.16	1.04	21.27	1.42	20.99	1.18
MnO	0.20	0.08	0.18	0.08	0.16	0.08
MgO	5.58	0.17	6.42	0.56	6.95	0.40
CaO	0.08	0.08	0.62	0.16	0.13	0.08
Na_2O	0.34	0.24	0.48	0.21	0.86	0.19
K_2O	9.07	0.45	3.66	1.33	2.60	0.72
$(NH_4)_2O$*	0.55	0.28	3.37	0.57	3.77	0.82
$(NH_4)_2O$†			2.60			
Total‡	96.21	0.83	95.62	0.84	96.11	2.53
Si	2.72	0.04	2.67	0.35	2.78	0.05
^{IV}Al	1.28	0.04	1.33	0.35	1.22	0.05
^{VI}Al	0.43	0.05	0.42	0.35	0.54	0.06
Ti	0.25	0.02	0.22	0.03	0.13	0.02
Fe^{2+}	1.34	0.07	1.33	0.09	1.27	0.04
Mn	0.01	0.01	0.01	0.00	0.01	0.01
Mg	0.63	0.02	0.71	0.35	0.75	0.04
$S_{oct.}$	2.67	0.04	2.70	0.34	2.70	0.05
Ca	0.01	0.01	0.04	0.01	0.01	0.01
Na	0.05	0.04	0.07	0.03	0.12	0.03
K	0.88	0.05	0.35	0.13	0.24	0.10
NH_4*	0.07	0.04	0.55	0.14	0.63	0.11

Notes: In parentheses (number of analyses).
* Calculated values.
† Estimated from the elemental analysis of N in golden mica separate from sample MP-1.
‡ Estimated, in the case of the AEM data, from the H_2O content deduced from the thermal curves.

TABLE 5. Representative analyses for retrogressive phases

	Fig. 1c				Figs. 1d and 5b		
	1	2	3	4	5	6	7
	Sm	Chl	Chl	Chl	Sm	Chl/Vrm	Chl/Vrm
SiO_2	43.49	31.04	30.00	29.44	44.90	32.41	31.23
Al_2O_3	25.56	22.41	21.50	21.73	31.10	21.08	21.59
TiO_2	1.02	0.00	0.00	0.00	0.27	0.28	0.59
FeO	8.91	26.58	26.49	26.16	2.27	25.56	27.16
MnO	0.07	0.47	0.00	0.00	0.00	0.40	0.00
MgO	1.87	7.47	6.83	7.36	1.26	8.61	5.99
CaO	0.31	0.27	0.57	0.65	0.94	0.34	0.28
Na_2O	0.26	0.00	0.00	0.97	0.00	0.00	0.44
K_2O	2.44	0.29	0.29	0.58	1.86	1.67	2.26
Total	83.94	88.54	85.67	86.88	82.58	90.34	89.53
Si	3.27	3.20	3.20	3.12	3.27	2.57	2.54
^{IV}Al	0.73	0.80	0.80	0.88	0.73	1.43	1.46
^{VI}Al	1.54	1.92	1.91	1.83	1.94	0.55	0.61
Ti	0.06	0.00	0.00	0.00	0.01	0.02	0.04
Fe^{2+}	0.56	2.29	2.36	2.32	0.14	1.70	1.85
Mn	0.01	0.04	0.00	0.00	0.00	0.03	0.00
Mg	0.21	1.15	1.09	1.16	0.14	1.02	0.73
Oct.	2.37	5.39	5.36	5.31	2.22	3.31	3.22
Ca	0.02	0.03	0.07	0.07	0.07	0.03	0.02
Na	0.04	0.00	0.00	0.20	0.00	0.00	0.07
K	0.24	0.04	0.04	0.08	0.17	0.17	0.23
Na + K + Ca	0.30	0.07	0.10	0.35	0.25	0.20	0.33
O	11	14	14	14	11	11	11

Notes: Retrogressive phases from sample MP-1-5 (Fig. 1c) mainly consist of "chloritic" grains. Their formulae have been calculated for 14 O, although some analyses contain important amounts of Na + K + Ca. In contrast, retrogressive phases from sample RMP1-1 (Fig. 1d) are more "vermiculitic." Their formulae have been calculated for 11 O, although the contribution of chlorite on the octahedral occupancy is evident.

TABLE 6. EMPA data for suhailite

	1	2	3	4	5	6	7	8	9	10	11	12	13	14	15	Average	σ
SiO_2	34.60	34.80	34.31	34.51	35.61	35.31	33.86	34.96	35.55	35.85	35.66	35.35	36.07	36.14	36.33	35.31	0.71
Al_2O_3	20.39	19.98	20.11	18.97	19.43	19.91	17.57	18.78	19.54	19.51	19.07	18.33	19.43	18.78	19.95	19.38	0.74
TiO_2	4.03	4.08	4.00	4.86	4.02	3.25	2.55	4.11	3.85	5.01	4.07	3.90	4.00	3.70	3.10	3.96	0.61
Cr_2O_3	0.00	0.00	0.00	0.00	0.00	0.00	0.00	0.00	0.01	0.00	0.00	0.00	0.00	0.01	0.00	0.00	0.01
NiO	0.05	0.10	0.14	0.19	0.06	0.05	0.04	0.04	0.02	0.03	0.04	0.00	0.06	0.00	0.03	0.05	0.05
FeO	19.27	20.34	18.92	21.09	20.58	21.52	25.80	20.56	19.66	18.84	19.77	19.57	19.14	19.09	20.88	20.21	1.69
MnO	0.17	0.16	0.16	0.15	0.17	0.16	0.20	0.19	0.19	0.12	0.27	0.19	0.14	0.16	0.16	0.17	0.03
MgO	7.53	7.60	6.96	6.76	6.69	5.89	5.60	7.30	6.77	6.11	6.61	7.60	6.90	7.61	5.21	6.65	0.80
CaO	0.40	0.40	0.45	0.79	0.23	0.36	0.42	0.31	0.28	0.37	0.20	0.49	0.59	0.63	0.23	0.39	0.17
Na_2O	0.96	0.92	0.92	0.58	0.72	1.10	0.67	1.21	0.96	1.13	0.88	0.14	0.48	0.12	0.93	0.79	0.31
K_2O	2.85	2.62	2.55	2.30	6.23	5.14	4.18	3.43	5.67	5.27	5.90	5.69	5.60	5.11	6.65	4.83	1.62
$(NH_4)_2O$	0.87	0.85	1.55	0.57	0.72	0.79	0.78	0.55	0.56	0.89	0.81	0.99	0.54	0.70	0.68	0.79	0.24
Cl	0.34	0.37	0.47	0.20	0.14	0.21	0.25	0.28	0.18	0.25	0.13	0.20	0.13	0.15	0.24	0.23	0.09
Total	91.12	91.85	90.07	90.78	94.47	93.50	91.67	91.45	93.05	93.14	93.29	92.27	92.97	92.05	94.15	92.53	1.30
Si	2.66	2.66	2.67	2.68	2.70	2.71	2.71	2.71	2.72	2.73	2.73	2.73	2.75	2.77	2.77	2.71	0.03
^{IV}Al	1.34	1.34	1.33	1.32	1.30	1.29	1.29	1.29	1.28	1.27	1.27	1.27	1.25	1.23	1.23	1.29	0.03
^{VI}Al	0.51	0.47	0.51	0.42	0.44	0.51	0.37	0.42	0.48	0.47	0.45	0.40	0.49	0.47	0.57	0.47	0.05
Ti	0.23	0.24	0.23	0.28	0.23	0.19	0.15	0.24	0.22	0.29	0.23	0.23	0.23	0.21	0.18	0.23	0.03
Cr	0.00	0.00	0.00	0.00	0.00	0.00	0.00	0.00	0.01	0.00	0.00	0.00	0.00	0.01	0.00	0.00	0.00
Ni	0.00	0.01	0.01	0.01	0.00	0.00	0.00	0.00	0.00	0.00	0.00	0.00	0.00	0.00	0.00	0.00	0.00
Fe^{2+}	1.24	1.30	1.23	1.37	1.31	1.38	1.73	1.33	1.26	1.20	1.27	1.26	1.22	1.22	1.33	1.30	0.13
Mn	0.01	0.01	0.01	0.01	0.01	0.01	0.01	0.01	0.01	0.01	0.02	0.01	0.01	0.01	0.01	0.01	0.00
Mg	0.86	0.87	0.81	0.78	0.76	0.67	0.67	0.84	0.77	0.69	0.76	0.88	0.78	0.87	0.59	0.76	0.09
Σoct	2.86	2.89	2.80	2.89	2.76	2.77	2.93	2.86	2.75	2.67	2.73	2.78	2.74	2.79	2.68	2.78	0.09
Ca	0.03	0.03	0.04	0.07	0.02	0.03	0.04	0.03	0.02	0.03	0.02	0.04	0.05	0.05	0.02	0.03	0.01
Na	0.14	0.14	0.14	0.09	0.11	0.16	0.10	0.18	0.14	0.17	0.13	0.02	0.07	0.02	0.14	0.12	0.05
K	0.28	0.26	0.25	0.23	0.60	0.50	0.43	0.34	0.55	0.51	0.58	0.56	0.54	0.50	0.65	0.47	0.16
NH_4	0.15	0.15	0.28	0.10	0.13	0.14	0.14	0.10	0.10	0.16	0.14	0.18	0.10	0.12	0.12	0.14	0.04
Σint	0.61	0.58	0.71	0.48	0.85	0.84	0.71	0.65	0.82	0.86	0.87	0.80	0.76	0.69	0.92	0.76	0.14

contrast, suhailite grains are characterized by the presence of small rutile inclusions with elongation parallel to the mica 001 plane (Fig. 11a). The SAED patterns show a general periodicity of ~10.20 Å and are characteristic of polytypes with variable stacking disorder. The perimeters of the golden mica grains show occasional signs of alteration, with the presence of Fe-oxide (Fig. 11b), similar to those described by Murakami et al. (2003) in weathered biotite. The AEM data consistently yielded

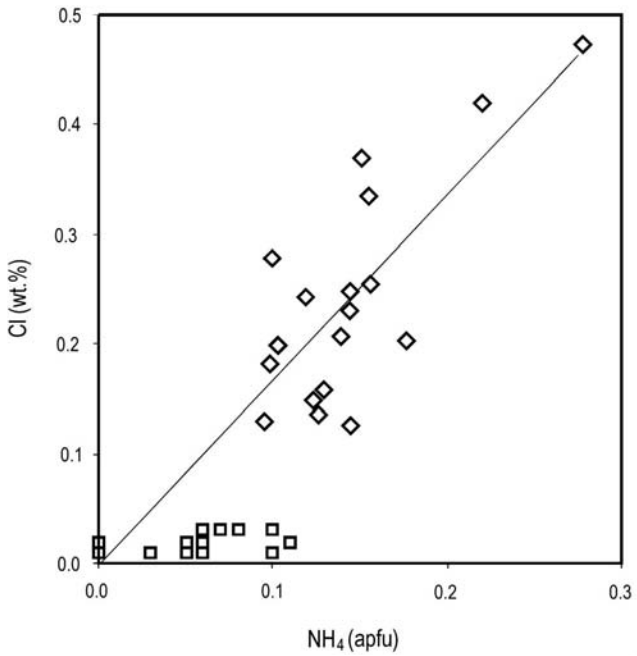

FIGURE 9. Chlorine (wt%) vs. NH_4 (apfu) plot, showing the low Cl content in red annite (squares) and the positive correlation between Cl and NH_4 in suhailite (diamonds).

intermediate compositions, indicating that golden mica grains contain both NH_4 and K. In some areas, small NH_4- and K-enriched domains show semi-coherent boundaries, as indicated by the Fourier transform image (Fig. 12a). Suhailite grains are typically characterized by the presence of abundant broad and discontinuous light fringes, grouped in subparallel bands of about 200 Å in thickness, which are tilted with respect to the plane (001), as observed in Figure 12b. This texture resembles the domainal one described in intermediate Na-K and Na-Ca micas (Livi et al. 1997; Ruiz Cruz 2008), and the exsolution textures in wonesite described by Veblen (1983). The HRTEM images indicate that disordered stacking sequences predominate in suhailite, showing frequent changes in orientation of layers, curvature of layers, and planar defects (Fig. 13). The more ordered areas display, however, sequences characteristic of 1-layer polytype, with lack of chlorite or vermiculite layers (Fig. 13, inset). The average formula of suhailite grains, deduced from the AEM data, is also shown in Table 4.

The compatibility index ($1 - K_P/K_C$), which is an estimation of the agreement between the physical properties (mean refractive index and density) and the chemical composition (Mandarino 2007), is 0.035 (excellent) when the chemical composition deduced from the EDX analyses is used, and 0.003 (superior) when the AEM data are used.

Thermal data

Differential thermal analysis and thermogravimetry (DTA-DTG-TG), obtained from suhailite enriched separates from sample MP-1M, were performed with a Netzsch STA 409 PE apparatus, using platinum/rhodium thermocouples and platinum crucibles. The following experimental conditions were used: sample weight = 15 mg, temperature range = 20–1020 °C, heating rate = 10°/min; reference Al_2O_3; static air atmosphere. The

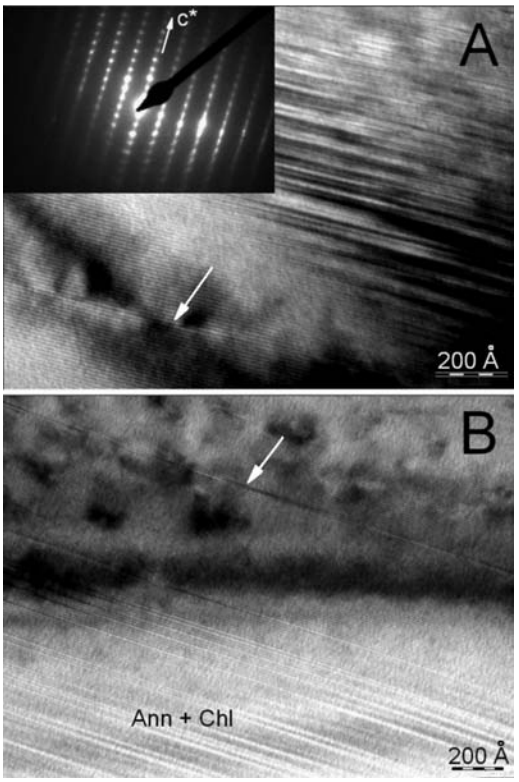

FIGURE 10. Lattice-fringe images of unaltered annite (**a**) and annite partially retrograded to chlorite (**b**). The SAED pattern (inset in **a**) corresponds to one-layer ordered polytype. Arrows mark the cleavage planes.

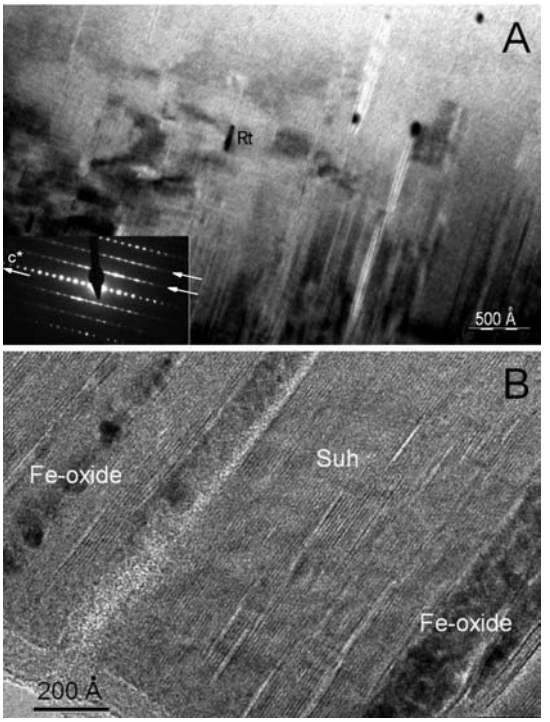

FIGURE 11. Lattice-fringe images of suhailite showing the presence of small rutile inclusions aligned along the 001 plane of mica (**a**) and the presence of Fe-oxide areas in a slightly retrograded suhailite grain (**b**). The SAED pattern (inset in **a**) corresponds to one-layer polytype with some stacking disorder, as indicated the streaking of the 0*kl* reflection rows parallel to **c*** (arrows).

DTA curve shows a low-temperature endothermic effect at 82 °C, due to the loss of absorbed water, and two adjacent endothermic effects at 502 and 680 °C (Table 7; Fig. 14). The first one is interpreted, as in the case of tobelite (Higashi 1982), as due to the NH_4 detachment, although NH_4 loss in tobelite begins at about 530 °C. The second one, due to suhailite dehydroxilation, occurs at temperatures higher than in tobelite, and notably lower than in biotite (Mackenzie 1970). The mass loss associated with the endothermic effect at 502 °C (2.52 wt%) can be used for estimating the average NH_4 content in suhailite + annite whereas the mass loss associated to the 680 °C endothermic effect (2.11 wt%) indicates the structural water content.

Infrared data

FTIR spectra were used for systematically testing the presence of NH_4 (Busigby et al. 2003). Spectra were recorded in KBr pellets (2 wt% samples) using a Nicolet spectrometer (20SXB) with a DTGS detector, in the range 4000–400 cm^{-1} (Málaga University). Resolution was 2 cm^{-1}. Four hundred scans were accumulated to improve the signal to noise ratio in the spectra.

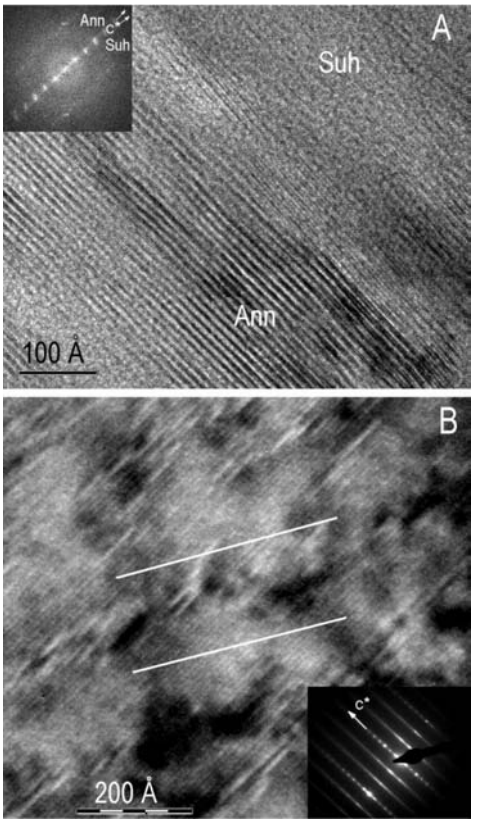

►**FIGURE 12.** (**a**) Lattice-fringe image showing a semi-coherent boundary between small annite- and suhailite-enriched domains. The Fourier transform image shows 00*l* reflections with two periodicities (~10 and ~10.25 Å), corresponding to annite and suhailite. (**b**) Lattice-fringe image showing sub-parallel bands, oblique to 001, of mica with uniform periodicity and mica with light broad fringes, interpreted as corresponding to annite- and suhailite domains.

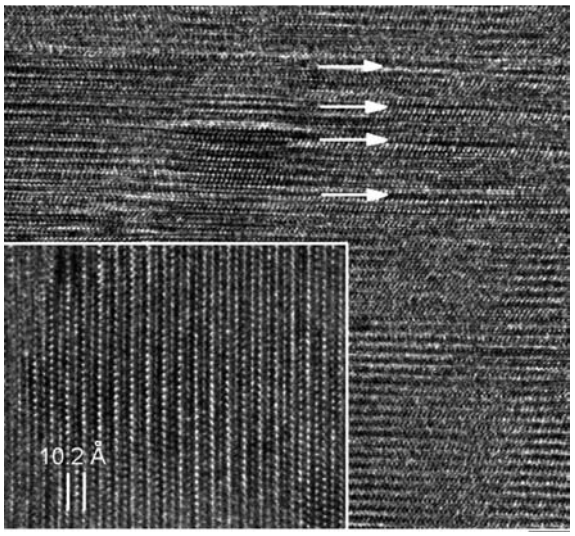

FIGURE 13. High-resolution image of suhailite showing local broadening of fringes, bending of layers associated with layer terminations, stacking disorder and planar defects (arrows) almost regularly spaced. Inset: Ordered area of suhailite showing regular stacking of layers with complete interlayer occupancy.

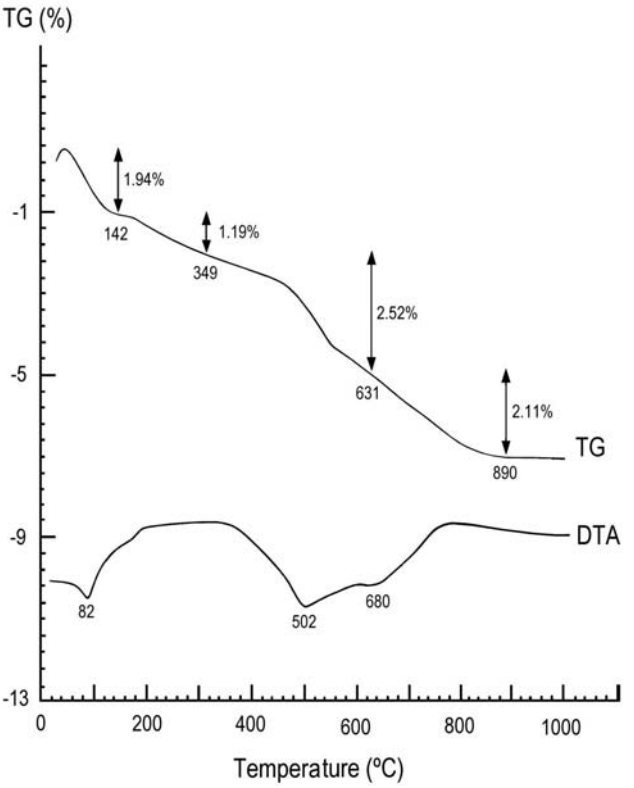

FIGURE 14. TG and DTA curves of a suhailite-enriched sample (MP-1M). The mass loss measured at the main intervals defined by the DTG curve (not shown) have been marked on the TG curve. For explanation see text and Table 7.

TABLE 7. Position of the endothermic effects in suhailite-enriched separate

Temperature (°C)	
82	Loss of adsorbed water
502	NH_4 detachment
680	Dehydroxilation

To avoid grinding effects in the preparation of the disk, samples and KBr were gently mixed manually. The spectra of suhailite-enriched separates always indicate the presence of quartz. The spectra show three main groups of mica bands (Table 8; Fig. 15): The OH-stretching vibration bands (at 3695, 3676, and 3659 cm^{-1}), the two first similar to those present in the spectrum of synthetic NH_4-phlogopite (Harlov et al. 2001); the vacancy bands (at 3620, 3595, and 3569 cm^{-1}), similar to those described in typical biotite (Farmer 1974); and the NH_4 bands. These appear in the spectra of unaltered samples at 2926, 2830, 1465, and 1430 cm^{-1}, as also found in tobelite (Higashi 1982), synthetic tobelite (Sucha et al. 1998) and synthetic NH_4-phlogopite (Harlov et al. 2001). Nevertheless, some other samples show a second band at ~1500 cm^{-1}. This value is similar to that found in some ammonium halides, and could be interpreted as due to shortening of the H-bridges in NH_4 coordinated to water molecules (Russell and White 1988), present in the hydrated mica (with basal spacing ~11 Å). This band also could indicate that retrogressive vermiculite contains some NH_4 in the interlayer.

ORIGIN

Suhailite is observed here to be a mineral formed under metamorphic temperature and pressure conditions. Textural data suggest that unoriented suhailite-bearing grains formed from primary red annite during the annite to fibrolite transformation. Indeed, graphite inclusions in suhailite maintain generally the same orientation as observed in the precursor annite (Fig. 6a). Formation of suhailite from annite with lower NH_4 and Cl contents would explain the enrichment of suhailite in both NH_4 and Cl. Two hypotheses seem acceptable for explaining the textures observed by TEM: (1) Segregation of K and NH_4, during growth of golden mica, leading to small domains of suhailite and annite; and (2) NH_4-enriched annite formed during the annite to fibrolite transformation, and then exsolved during cooling to produce K- and NH_4-enriched domains. If the first hypothesis is considered, the presence of K- and NH_4-enriched domains could be an indication of microscale variations in the K/NH_4 ratio in the pores of the rocks during the formation of the mica, which led to variation in NH_4 content in the mica. Although this hypothesis cannot be discarded, the presence of NH_4-enriched regular microdomains, oblique to the basal planes (Fig. 12b), suggests that these formed by exsolution, through diffusion of K^+ and NH_4^+ parallel to the layers. The presence of minute rutile inclusions in suhailite also suggests that Ti was expelled from the mica structure during suhailite growth.

The origin of the NH_4 can be related to the high organic matter content in the original sediment, as also indicated by the high graphite content (Table 3) and the presence of relics of tobelite in the overlying schists (Ruiz Cruz and Sanz de Galdeano 2008). Although the age of primary annite is uncertain, textures suggest that it is the older mica generation present in the rocks. Based on a Paleozoic or pre-Paleozoic age for these formations suggested by Egeler and Simons (1969), and a Hercynian-age metamorphic episode (Zeck and Whitehouse 1999, 2002), it is likely that the

TABLE 8. Infrared bands (cm^{-1}) in suhailite-enriched separates

Hydroxyl stretching vibrations	Vacancy bands	NH_4 bands
3695 (s)	3620 (s)	2926 (w)
3676 (w)	3595 (w)	2830 (w)
3659 (m)	3569 (w)	1509 (w)
		1465 (sh)
		1430 (w)

Notes: s = strong; m = medium; w = weak; sh = shoulder.

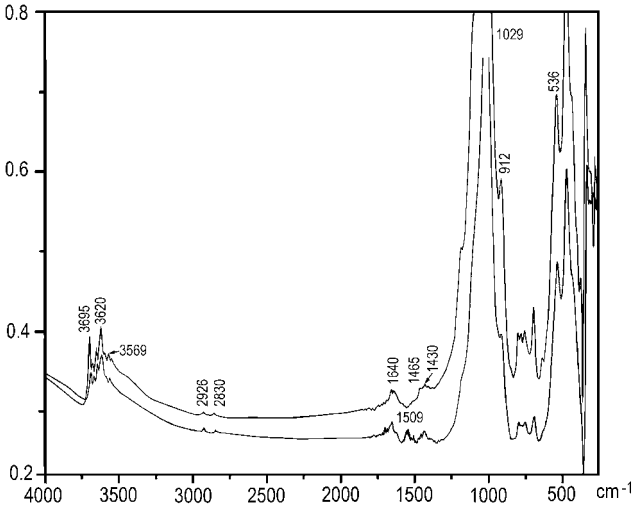

FIGURE 15. FTIR spectra of two suhailite-rich samples (upper = MP-1M; lower = MP1-3). For explanation see text and Table 8.

age of the ammonium-bearing annite is Hercynian or older. The presence of suhailite in gneisses clearly indicates that ammonium-bearing micas are stable phases up to at least 500 °C.

ACKNOWLEDGMENTS

The authors are grateful to P. Schroeder, E. Daniels, and H. Lindgreen, whose suggestions and corrections have notably improved the manuscript; to F. Fontan (recently deceased) for determining the refractive indices. Also to M.M. Abad (Universidad de Granada), and to J.L. Baldonedo and A. Gómez (Universidad Complutense) for help in obtaining TEM/AEM data, and to M. Bentabol for the realization of the FTIR spectra. This study has received financial support from the Project CGL 2006-02481 (Ministerio de Educación y Ciencia) and from the Research Group RNM-199 (Junta de Andalucía).

REFERENCES CITED

Azañón, J.M., Crespo-Blanc, A., and García-Dueñas, V. (1997) Continental collision, crustal thinning, and nappe forming during the pre-Miocene evolution of the Alpujárride Complex (Alboran Domain, Betics). Journal of Structural Geology, 19, 1055–1071.

Boss, A., Duit, W., van der Eerden, A.J., and Jansen, J.B. (1988) Nitrogen storage in biotite: An experimental study of the ammonium and potassium partitioning between 1M-phlogopite and vapour at 2 kb. Geochimica et Cosmochimica Acta, 52, 1275–1283.

Busigby, V., Cartigny, P., Philippot, P., and Javoy, M. (2003) Ammonium quantification in muscovite by infrared spectroscopy. Chemical Geology, 198, 21–31.

Cliff, G. and Lorimer, G.W. (1975) The quantitative analysis of thin specimens. Journal of Microscopy, 103, 203–207.

Daniels, E.J. and Altaner, S.P. (1990) Clay mineral authigenesis in coal and shale from the Anthracite region, Pennsylvania. American Mineralogist, 75, 825–839.

Drits, V.A., Lindgreen, H., and Salyn, A.L. (1997) Determination of the content and distribution of fixed ammonium in illite-smectite by X-ray diffraction; application to North Sea illite-smectite. American Mineralogist, 82, 79–87.

Drits, V.A., Sakharov, B.A., Salyn, Al.L., and Lindgreen, H. (2005) Determination of the content and distribution of fixed ammonium in illite-smectite using a modified X-ray diffraction technique: Application to oil source rocks of western Greenland. American Mineralogist, 90, 71–84.

Egeler, C.G. and Simon, O.J. (1969) Sur la tectonique de la Zone Bétique (Cordillères Bétiques, Espagne). Verhandelingen der Koninklijke Nederlandse Akademie van Wetenschappen, 25-3, 90 p. North-Holland Publishing Company, Amsterdam.

Eugster, H.P. and Muñoz, J. (1966) Ammonium micas: Possible sources of atmospheric ammonia and nitrogen. Science, 151, 683–686.

Farmer, V.C. (1974) The layer silicates. In V.C. Farmer, Ed., The Infrared Spectra of Minerals, p. 331–365. Mineralogical Society, London.

García-Casco, A., Sánchez-Navas, A., and Torres-Roldán, R.L. (1993) Disequilibrium decomposition and breakdown of muscovite in high *P-T* gneisses, Betic alpine belt (southern Spain). American Mineralogist, 78, 158–177.

Guidotti, C.V. (1984) Micas in metamorphic rocks. In S.W. Bailey, Ed., Micas, 13, p. 357–467. Reviews in Mineralogy, Mineralogical Society of America, Chantilly, Virginia.

Harlov, D.E., Andrut, M., and Melzer, S. (2001) Characterization of NH_4-phlogopite $(NH_4)(Mg_3)(AlSi_3O_{10})(OH)_2$ and ND_4-phlogopite $(ND_4)(Mg_3)(AlSi_3O_{10})(OD)_2$ using IR spectroscopy and Rietveld refinement of XRD spectra. Physic and Chemistry of Minerals, 28, 77–86.

Higashi, J. (1982) Tobelite, a new ammonium dioctahedral mica. Mineralogical Journal, 11, 138–146.

Honma, H. (1996) High ammonium contents in the 3800 Ma Isua supracrustal rocks, central West Greenland. Geochimica et Cosmochimica Acta, 60, 2173–2178.

Honma, H. and Itihara, Y. (1981) Distribution of ammonium in minerals of metamorphic and granitic rocks. Geochimica et Cosmochimica Acta, 45, 983–988.

Juster, T.C., Brown, P.E., and Bailey, S.W. (1987) NH_4-bearing illite in very low grade metamorphic rocks associated with coal, northeastern Pennsylvania. American Mineralogist, 72, 555–565.

Kretz, R. (1983) Symbols for rock-forming minerals. American Mineralogist, 68, 277–279.

Livi, K.J.T., Veblen, D.R., Ferry, J.M., and Frey, M. (1997) Evolution of 2:1 layered silicates in low-grade metamorphosed Liassic shales of Central Switzerland. Journal of Metamorphic Geology, 15, 323–344.

Mackenzie, R.C. (1970) Simple phyllosilicates based on gibbsite- and brucite-like sheets. In R.C. Mackenzie, Ed., Differential Thermal Analysis, 1, p. 498–538. Academic Press, London.

Mandarino, J.A. (2007) The Gladstone-Dale compatibility of minerals and its use in selecting mineral species for further study. Canadian Mineralogist, 45, 1307–1324.

Martin, J.D. (2004) Using XPowder: A software package for Powder X-Ray diffraction analysis, 105 p. D.L. GR 1001/04, Spain, www.xpowder.com.

Marukami, T., Utsunomiya, S., Yokoyama, T., and Kasama, T. (2003) Biotite dissolution processes and mechanisms in the laboratory and in nature: Early stage weathering environment and vermiculitization. American Mineralogist, 88, 377–386.

Mingram, B. and Braüer, K. (2001) Ammonium concentration and nitrogen isotope composition in metasedimentary rocks from different tectonometamorphic units of the European Variscan Belt. Geochimica et Cosmochimica Acta, 65, 273–287.

Nieto, F. (2002) Characterization of coexisting NH_4- and K-micas in very low-grade metapelites. American Mineralogist, 87, 205–216.

Ruiz Cruz, M.D. (2008) Na-bearing white micas from Triassic rocks of the transition between Maláguide and Alpujárride Complexes (Betic Cordillera, Spain). Clays and Clay Minerals, 56, 344–358.

Ruiz Cruz, M.D. and Sanz de Galdeano, C. (2008) High-temperature ammonium white mica from the Betic Cordillera (Spain). American Mineralogist, 93, 977–987.

Russell, J.D. and White, J.L. (1988) Infrared study of the thermal decomposition of ammonium rectorite. Clays and Clay Minerals, 14, 181–191.

Schroeder, P.A. and Ingall, E.D. (1994) A method for the determination of nitrogen in clays, with application to the burial diagenesis of shales. Journal of Sedimentary Research, A64, 694–697.

Sucha, V., Elsass, F., Eberl, D.D., Kuchta, L., Madejova, J., Gates, W.P., and Komadel, P. (1998) Hydrothermal synthesis of ammonium illite. American Mineralogist, 83, 58–67.

Veblen, D.R. (1983) Exsolution and crystal chemistry of the sodium mica wonesite. American Mineralogist, 68, 554–565.

Vedder, W. (1964) Correlations between the infrared spectrum and chemical composition of mica. American Mineralogist, 49, 736–768.

Zeck, H.P. and Whitehouse, M. (1999) Hercynian, Pan-African, Proterozoic and Archean ion-microprobe zircon ages for a Betic-Rif core complex, Alpine belt, W Mediterranean—consequences for its *P-T-t* path. Contributions to Mineralogy and Petrology, 134, 134–149.

——— (2002) Repeated age resetting in zircons from Hercynian-Alpine polymetamorphic schists (Betic-Rif tectonic belt, S. Spain). Chemical Geology, 182, 275–292.

MANUSCRIPT RECEIVED APRIL 25, 2008
MANUSCRIPT ACCEPTED SEPTEMBER 16, 2008
MANUSCRIPT HANDLED BY PAUL SCHROEDER